HODGKIN HUXLEY MODEL AND BIFURCATIONS IN THE MORRIS-LECAR MODEL

BY

SHIYI LYU

A Thesis Submitted to the Graduate Faculty of

WAKE FOREST UNIVERSITY GRADUATE SCHOOL OF ARTS AND SCIENCES

in Partial Fulfillment of the Requirements

for the Degree of

MASTER OF SCIENCE

Mathematics

August, 2024

Winston-Salem, North Carolina

Approved By:

Miaohua Jiang, Ph.D., Advisor

Jennifer Erway, Ph.D., Chair

Fan Yang, Ph.D.

acknowledgments

There are many people who helped to make this thesis possible. I want to thank Dr Mayle and Dr Erway especially, since I skipped classes to finish this thesis, and they are not mad at me at all. And I also want to thank Dr Jiang, since he never give up on me. The last person I want to thank to is Dr Yang, he helped me a lot with this thesis. I acknowledge the use of ChatGPT in the exposition part of this thesis.

Table of Contents

Abstract

This thesis examines mathematical models in neuroscience, focusing on the Hodgkin-Huxley and Morris-Lecar models to understand the dynamics of neuronal activities. It explores the voltage-clamp technique pivotal for understanding ionic currents across neuronal membranes, leading to groundbreaking insights into how action potentials are initiated and propagated. With a detailed analysis, this thesis dissects these foundational models, introducing modifications that align more closely with observed biological phenomena. By employing bifurcation theory, it examines the transition between different neuronal firing patterns, providing a rich theoretical framework for understanding the complex behaviors of neurons under various stimuli.

Chapter 1: Introduction

As an animal species on Earth, human brains do not count as 'big'. Neuroscientists figured out that both human and giant squid neurons share fundamental characteristics, but there are notable differences. One key distinction is size: giant squid neurons, particularly their axons, are much larger than human neurons. Additionally, the specific ion channels and mechanisms within these neurons may vary, but the basic principles of neuronal function are similar. These wrap up the reason neuroscientists use giant squid to learn about neurons related to human beings.

In this thesis, we first introduce The Hodgkin-Huxley Model in Chapter 2, , which was a groundbreaking development in the understanding of ionic currents across the neuronal membrane and the generation of action potentials. Alan Hodgkin and Andrew Huxley conducted experiments with the giant axon of the squid, where they utilized the voltage-clamp technique to measure the ionic currents during action potentials, which contributed to identifying the voltage-gated ion channels. The chapter explains the mathematical formulation of the model, expressing the ionic current as a product of the membrane capacitance and the change in membrane potential over time. It describes the model in the context of a cylindrical cell and introduces the concept of cable modeling, which simplifies the representation of the neuron as a cable with certain electrical properties. Furthermore, the Hodgkin-Huxley model's detailed account of potassium and sodium conductances as functions of membrane potential and time is discussed, emphasizing their role in neuron excitability. The model showcases the dynamic interaction of these ions with gating variables, leading to a mathematical framework that profoundly impacts our understanding of neural electrical behavior. Then we delve into the Morris-Lecar model, a simplification of the Hodgkin-Huxley model that focuses on a two-variable system to describe the elec-

trical activity in neurons. This model incorporates both calcium and potassium ions and is adapted to capture the dynamics of cells where calcium conductance is crucial in generating action potentials. The chapter provides a comprehensive overview of the Morris-Lecar model's equations, detailing the interplay between the membrane potential and ionic currents. It outlines the biological significance of parameters such as ion conductances and equilibrium potentials and elaborates on how the model can be used to understand the neuron's response to stimuli and simulate its behavior.

Then in chapter 3, we explore the bifurcations in the Morris-Lecar model, focusing on two types: Hopf and Saddle-Node on Limit Cycle (SNLC). It discusses how these bifurcations provide insights into the transitions between different neuronal firing patterns, such as from rest to repetitive firing, and from one rhythmic pattern to another. The chapter also introduces the process of finding equilibrium points and their stability. After that, we find the specific value where the bifurcation occurs and study the phase diagrams near the bifurcation values.

In the last chapter, we emphasize how these mathematical frameworks have advanced our capacity to develop targeted treatments for neurological disorders by precisely simulating the neuronal response to pharmaceutical compounds. Furthermore, the models inform the design of prosthetics and interfaces that simulate neuronal behavior, promising to revolutionize how we interact with machines and augment human capabilities. The insights garnered from these models also deepen our understanding of pathological changes in neuronal dynamics, which can pave the way for novel therapeutic strategies.

Chapter 2: Hodgkin-Huxley Model and Morris-Lecar Model

The development of the Hodgkin-Huxley model began with experiments conducted by Hodgkin and Huxley in the late 1940s and early 1950s. They inserted microelectrodes into the giant axon of the squid, a choice made due to the unusually large size of these axons, which facilitated the insertion of electrodes and precise measurement of the electrical activity. Through a series of intricate experiments, they were able to measure the ionic currents that flow in and out of the neuron during the generation and propagation of action potentials.

From a mathematical perspective, the current passing through the lipid bilayer is expressed as $I_C = C_M \cdot \frac{\partial V_M}{\partial t}$, where I_C is the total capacitance current and C_M is the membrane capacitance and V_M here is the membrane potential. Therefore from this, we have capacitance per unit area: $i_c = c_M \cdot \frac{\partial V_M}{\partial t}$.

For now, we consider the cell in the shape of a long cylinder, with radius a and length x, just like Figure 2.1.

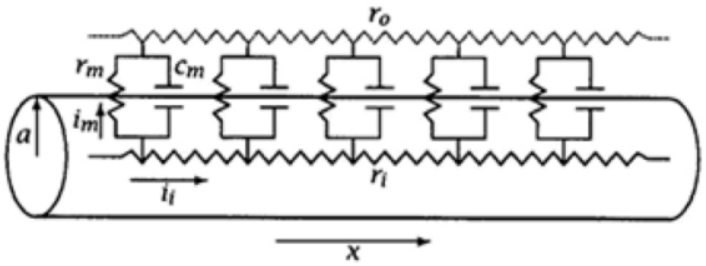

Figure 2.1: Cable Modeling [3]

Here in Figure 2.1, r_o represents the resistance of the extracellular space, r_i repre-

sents resistance of the cytoplasm, r_m represents membrane resistance, c_m represents membrane capacitance, i_m represents the current across the membrane, i_i represents current along inside the cable. The cable equation is a partial differential equation that describes how the membrane potential $V_M(x,t)$ depends on currents entering, leaving, and flowing within the neuron. We first consider the axial current flowing along the neuron due to voltage gradients. Let r_L be the specific intracellular resistivity, which is the constant of proportionality, therefore the total resistance of the cable with radius a and length Δx is $R_L = \frac{r_L \Delta x}{\pi a^2}$.

The Ohm's Law states that the electric current through a conductor between two points is directly proportional to the voltage across the two points. Therefore, we have $V = IR$ where I is the current through the conductor, V is the voltage measured across the conductor and R is the resistance of the conductor. [6] Then the cable equation follows from Ohm's law that at any point x, the decrease in V_M with distance is equal to the current times the resistance.

$$V_M(x+\Delta x,t) - V_M(x,t) = -I_i(x,t)R_L = -I_i(x,t)\frac{r_L \Delta x}{\pi a^2}.$$

The presence of a minus sign follows the convention that a positive current represents the flow of positive charges moving from left to right. Consequently, when the voltage decreases as x increases, the resulting current is deemed positive. Letting $\Delta x \to 0$, we have

$$\lim_{\Delta x \to 0} V_M(x+\Delta x,t) - V_M(x,t) = V_M(x,t) - V_M(x,t) = 0,$$

$$\lim_{\Delta x \to 0} -I_i(x,t)\frac{r_L \Delta x}{\pi a^2} = 0, \text{ with L'Hopital's rule}$$

$$-\frac{r_L \Delta x}{\pi a^2}\frac{\partial V_M}{\partial x}(x,t) = I_i(x,t).$$

Let i_{ion} be the current per unit area due to ions flowing into and out of the cell. Then the total ionic current that flows across a membrane of radius a and length Δx

is given by

$$I_{ion} = (2\pi a \Delta x) i_{ion}.$$

Since we know that the total capacitance of a membrane is equal to the specific membrane capacitance multiplied by the total surface area of the membrane, with the cable radius a and length Δx, the total capacitance is given by $C_M = (2\pi a \Delta x) c_M$ and the quantity of current required to alter the membrane potential at a given rate of $\frac{\partial V_M}{\partial t}$ will become:

$$I_c(x,t) = (2\pi a \Delta x) \cdot c_M \cdot \frac{\partial V_M}{\partial t}.$$

With Kirchhoff's current law, we know that the total current entering a junction (or node) in an electrical circuit is equal to the total current leaving the junction. Therefore, we have

$$I_c(x,t) + I_{ion}(x,t) = -I_i(x + \Delta x, t) + I_i(x,t),$$

$$(2\pi a \Delta x) c_M \cdot \frac{\partial V_M}{\partial t} + (2\pi a \Delta x) i_{ion} = \frac{\pi a^2}{r_L} \frac{\partial V_M}{\partial t}(x + \Delta x, t) - \frac{\pi a^2}{r_L} \frac{\partial V_M}{\partial t}(x,t),$$

$$c_M \cdot \frac{\partial V_M}{\partial t} = \frac{\pi a}{2 r_L} \frac{\partial^2 V_M}{\partial x^2} - i_{ion}.$$

From step two to step three, we divide both sides by $2\pi a \Delta x$ and let $\Delta x \to 0$. Since within giant squid axon, $i_{ion} = i_K + i_{Na} + i_L$, we have the Hodgkin-Huxley model for an action potential on the squid's giant axon:

$$c_M \frac{\partial V_M}{\partial t} = \frac{a \partial^2 V_M}{2 r_L \partial x^2} - g_K (V_M - E_K) - g_{Na} (V_M - E_{Na}) - g_L (V_M - E_L),$$

where a is the fixed radius of the axon. The axon can be seen as a cylinder, so the membrane potential depends on the spatial variable x and time t. c_M is a specific membrane capacitance. g_K, g_{Na} and g_L are the membrane conductances. g_K and

g_{Na} are the voltage-gated conductances that change with time during an action potential, while g_L is the leak conductance. E_K and E_{Na} are the channel potentials for potassium and sodium and E_L is the leak reversal potential [3].

2.1 Voltage Clamped

The voltage clamp technique is a fundamental experimental method used in electrophysiology to study ionic currents across the membranes of neurons or other excitable cells. This method was crucial to the development of the Hodgkin-Huxley model, which describes how action potentials in neurons are initiated and propagated. In the early 1950s, Alan Hodgkin and Andrew Huxley assumed V is a constant in the neuron, which helped them to simplify the model.

By applying a voltage clamp to a neuron and then varying the membrane potential, Hodgkin and Huxley were able to deduce the existence of voltage-gated ion channels and described their dynamics mathematically. Their model explains how the flow of sodium and potassium ions through their respective channels generates the action potential, a rapid rise and fall in membrane potential that constitutes a fundamental signal in the nervous system.

2.1.1 Sodium Conductance

Sodium ions enter through the activation gates, and later exist through the inactivation gates. Potassium conductance remains at the peak until repolarization occurs. In contrast, sodium conductance spikes and then decreases during sustained depolarization. Hodgkin and Huxley theorized about the cause of this transient sodium behavior, recognizing the need for a mechanism in their model to reset conductance to baseline during prolonged depolarizations.

To determine the appropriate exponents for the activation (m) and inactivation

(h) variables, they applied a formula used for sodium, expressed as $g_{Na} = \overline{g_{Na}} m^p h^q$, with m and h controlling sodium inflow activation and inactivation, respectively, and $\overline{g_{Na}}$ are representing sodium's maximum conductance value. According to the data fitting, we have

$$g_{Na} = \overline{g_{Na}} m^3 h$$

which intuitively means that 3 activation gates and 1 inactivation gate must be open for the channel to be open.

For a better understanding of the expression of the rate, we have the gate model, which can be described as

$$C \underset{\beta(V)}{\overset{\alpha(V)}{\rightleftharpoons}} O,$$

where C and O represent closed and open states, and $\alpha(V)$ and $\beta(V)$ are the voltage-dependent rate constants at which a gate goes from the open to closed and closed to open states. To better understand, we need to use the Law of Mass Action, which is a principle in chemistry that quantifies the relationship between the reactants and products in a chemical reaction at equilibrium. It states that the rate of a reaction is directly proportional to the product of the concentrations (or activities) of the reactants, each raised to the power of its stoichiometric coefficient in the balanced chemical equation [11]. With this law, we have

$$\frac{\partial m}{\partial t} = \alpha(V)(1 - m) - \beta(V) \cdot m = \frac{m_\infty(V) - m}{\tau(V)},$$

where

$$m_\infty(V) = \frac{\alpha_m(V)}{\alpha_m(V) + \beta_m(V)} \quad \text{and} \quad \tau_m(V) = \frac{1}{\alpha_m(V) + \beta_m(V)}.$$

Here, m is the rate of open gates, then we have $1 - m$ as the rate of closed gates. To find $m(t)$ as a function and $m(0)$ as an initial condition, we first recognize that the

equation has a stable equilibrium solution at $m = m_\infty(V)$, where the rate of change $\frac{\partial m}{\partial t} = 0$. And then for initial deviation from the equilibrium, we use $m(0) - m_\infty(V)$ to represent. At $t = 0$, the exponential term is 1, and $m(0) = m_\infty(V) + (m(0) - m_\infty(V)) \cdot 1$, which simplifies to the initial condition $m(0)$. As t increases, the exponential term decreases towards zero, causing $m(t)$ to approach $m_\infty(V)$. The rate at which $m(t)$ approaches $m_\infty(V)$ is governed by $\tau(V)$, which is the time constant for the process. Therefore, to show how the difference between the initial condition $m(0)$ and the steady state $m_\infty(V)$ decreases over time, we use the exponential decay factor, which in this case is $e^{-t/\tau(V)}$. Thus, the solution starting at $m(0)$ is

$$m(t) = m_\infty(V) + (m(0) - m_\infty(V)) \cdot e^{-t/\tau_m}.$$

Borg-Graham[2] and colleagues proposed a straightforward model grounded in thermodynamics, positing that the probability of a channel opening or closing changes exponentially with the potential. Then we have

$$\alpha(V) = \alpha_0 \cdot e^{-(a_1 + b_1 \cdot V)/(RT)} \quad \text{and} \quad \beta(V) = \beta_0 \cdot e^{-(a_2 + b_2 \cdot V)/(RT)},$$

where R is the gas constant, T is the absolute temperature in degrees Kelvin, and a_1, a_2, b_1, and b_2 are constants specific for this transition. From this, we find that

$$m_\infty(V) = \frac{1}{1 + e^{-2 \cdot \frac{V - V_1}{V_2}}} = \frac{1}{2}[1 + \tanh((V - V_1)/V_2)],$$

where V_1, V_2 are constants.

Similarly, we have the statements for the inactivation of sodium channel,

$$h(t) = h_\infty(V) + (h(0) - h_\infty(V)) \cdot e^{-t/\tau_h},$$

where

$$h_\infty(V) = \frac{\alpha_h(V)}{\alpha_h(V) + \beta_h(V)} \quad \text{and} \quad \tau_h(V) = \frac{1}{\alpha_h(V) + \beta_h(V)}.$$

At this stage, Hodgkin and Huxley likely explored different combinations of the powers of m and h to achieve the correct profile for sodium conductance's increase. The conductance needed to exhibit a rise characterized by a single inflection point, followed by a decline without any inflection point. Base on Hodgkin and Huxley's experimental data that sodium and potassium channels have four gates each. Therefore their choice was to use $g_{Na} = \overline{g_{Na}} m^3 h$. This brings the sodium conductance formula to be [1]

$$g_{Na} = \overline{g_{Na}}(m_\infty - m_\infty e^{-\frac{t}{\tau_m}})^3 (h_0 e^{-\frac{t}{\tau_h}})$$

$$g_{Na} = \overline{g_{Na}}(m_\infty)^3 h_0 (1 - e^{-\frac{t}{\tau_m}})^3 e^{-\frac{t}{\tau_h}}.$$

2.1.2 Potassium Conductance

Hodgkin and Huxley developed a model to explain potassium conductance in neurons similarly to the previous section. As mentioned, potassium channels have four gates, which showing that it was proportional to the fourth power of a variable (n) governed by a first-order differential equation. This model links neuron excitation and action potential generation to membrane potential and ion concentrations across the membrane.

The established assumptions describing potassium conductance are:

$$g_K = \overline{g_K} n^4,$$

$$\frac{dn}{dt} = \alpha_n (1 - n) - \beta_n n.$$

The variable n represents the fraction of internal potassium transfer channels, while $1-n$ represents external channels. Essentially, n and $1-n$ can also be viewed as the probabilities of potassium channels being open for inward and outward transfer, respectively.

Without direct knowledge of the membrane's physical structure, Hodgkin and

Huxley introduced α_n and β_n as voltage-dependent rate constants for potassium ions moving in and out of the membrane, reflecting the dynamic balance of ion transfer rates. When the membrane is depolarized, an increase in α_n should occur if the particle carries a negative charge, while β_n should correspondingly decrease.

Hodgkin and Huxley thought of the K^+ channel as composed of 4 independent gates, each of which must be open for the channel to be open. Interpreting n as the probability to which a gate is open, their model implies that ion transfer across the membrane requires four gates to be open, This indicates that four gates are necessary for ion passage in a channel.

In the resting state, where $V = 0$, n has a resting value which is

$$n_0 = \frac{\alpha_{n_0}}{\alpha_{n_0} + \beta_{n_0}}.$$

When V undergoes an abrupt change, α_n and β_n immediately adjust to values corresponding to the new voltage. The function of $n(t)$ meets the initial condition of n equaling n_0 at $t = 0$:

$$n(t) = n_\infty(V) + (n(0) - n_\infty(V)) \cdot e^{-t/\tau_n},$$

where

$$n_\infty(V) = \frac{\alpha_n(V)}{\alpha_n(V) + \beta_n(V)} \quad \text{and} \quad \tau_n(V) = \frac{1}{\alpha_n(V) + \beta_n(V)}.$$

Similarly to sodium rate, we have

$$n_\infty(V) = \frac{1}{2}[1 + \tanh((V - V_3)/V_4)],$$

where V_3, V_4 are constants.

2.1.3 Voltage Clamped Hodgkin-Huxley Model

Using the voltage-clamp data, Hodgkin and Huxley derived expressions for the K^+ and Na^+ conductances. They let

$$g_K = \overline{g_K} n^4$$

$$g_{Na} = \overline{g_{Na}} m^3 h.$$

In the equation, $\overline{g_K}$ and $\overline{g_{Na}}$ are constants with the dimensions of conductance per square centimeter. n, m, and h are gating variables between 0 and 1. n represents the fraction of which one of the 4 gates opens. m represents the activation variable responsible for activating the carrying of sodium. h is the inactivation variable responsible for shutting down the inflow of sodium and restoring the resting levels.

So the total membrane current I as a function of time and voltage under voltage clamps situation [7]:

$$I = C_M \frac{dV}{dt} + \overline{g_K} n^4 (V - V_K) + \overline{g_{Na}} m^3 h (V - V_{Na}) + \overline{g_l}(V - V_l),$$

where

$$\frac{dn}{dt} = \alpha_n(1-n) - \beta_n n,$$

$$\frac{dm}{dt} = \alpha_m(1-m) - \beta_m m,$$

$$\frac{dh}{dt} = \alpha_h(1-h) - \beta_h h,$$

and

$$\alpha_n = 0.01 \cdot \frac{V+10}{\exp(\frac{V+10}{10}) - 1},$$

$$\beta_n = 0.125 \cdot \exp(\frac{V}{80}),$$

$$\alpha_m = 0.1 \cdot \frac{V+25}{\exp\frac{V+25}{10} - 1},$$

$$\beta_m = 4 \cdot \exp(\frac{V}{18}),$$

$$\alpha_h = 0.07 \cdot \exp(\frac{V}{20}),$$

$$\beta_h = \frac{1}{\exp(\frac{V+30}{10}) + 1},$$

where α_n, β_n, α_m, β_m, α_h and β_h are voltage-dependent rate constants that do not vary over time.

To construct the model of voltage-clamped Hodgkin-Huxley Model, we collected the data for the system. Here we have the chart for typical ion concentrations in cell [8],

Typical ion concentrations in cells			
Ion	Inside(mM)	Outside(mM)	Equilibrium potential(mV)
Frog muscle			T=20°C
K^+	124	2.25	$58 \cdot \log(\frac{2.25}{124}) = -101$
Na^+	10.4	109	$58 \cdot \log(\frac{109}{10.4}) = +59$
Cl^-	1.5	77.5	$-58 \cdot \log(\frac{77.5}{1.5}) = -99$
Ca^{2+}	10^{-4}	2.1	$29 \cdot \log(\frac{2.1}{10^{-4}}) = +125$
Squid axon			T=20°C
K^+	400	20	$58 \cdot \log(\frac{20}{400}) = -75$
Na^+	50	440	$58 \cdot \log(\frac{440}{50}) = +55$
Cl^-	40 - 150	560	$-58 \log(\frac{560}{40-150}) = -66$ to -33
Ca^{2+}	10^{-4}	10	$29 \cdot \log(\frac{10}{10^{-4}}) = +145$
Mammalian cell			T=37°C
K^+	140	5	$62 \cdot \log(\frac{5}{140}) = -89.7$
Na^+	5 - 15	145	$62 \cdot \log(\frac{145}{5\text{to}15}) = +90 - (+61)$
Cl^-	4	110	$-62 \log(\frac{110}{4}) = -89$
Ca^{2+}	10^{-4}	2.5 - 5	$31 \cdot \log(\frac{2.5-5}{10^{-4}}) = +136 - (+145)$

2.2 Space-Clamped

George Marmont [9], simplified the problem by eliminating space as a variable. His breakthrough involved achieving isopotentiality along the squid axon by threading a wire inside, short-circuiting longitudinal resistance. This method, called a space clamp, ensured a uniform potential across the axon's length, eliminating voltage gradients and propagation.

However, the space clamp [10], though groundbreaking, is now rarely used due to the prevalence of the "patch clamp" technique. The surface resistance of the axial wire remained a significant challenge in space clamping. If the membrane potential is maintained at a constant value, the capacitive current becomes zero.

Therefore, in this case, $\frac{\partial^2 V_M}{\partial x^2} = 0$, and

$$
\begin{aligned}
c_M \frac{dV}{dt} &= -\overline{g_K} n^4 (V - V_K) - \overline{g_{Na}} m^3 h (V - V_{Na}) - \overline{g_l}(V - V_l), \\
\frac{dn}{dt} &= \phi[\alpha_n(V) \cdot (1 - n) - \beta_n(V) \cdot n], \\
\frac{dm}{dt} &= \phi[\alpha_m(V) \cdot (1 - m) - \beta_m(V) \cdot m], \\
\frac{dh}{dt} &= \phi[\alpha_h(V) \cdot (1 - h) - \beta_h(V) \cdot h].
\end{aligned}
$$

Here we add the temperature factor for the system, where $\phi = Q_{10}^{(T - T_{base})/10}$ [3]. Understanding the significance of the experimental temperature is crucial, as the stochastic behavior of channels makes them temperature-sensitive. The likelihood of channels changing states is exponentially related to temperature, with higher temperatures accelerating the rate of switching.

For giant squid, the base temperature for the axon is $6.3°C$. As a temperature coefficient, $Q_{10} = 3$. Hodgkin and Huxley chose T as the average body temperature

for giant squid, which $T = 18.5°C$. They let $c_M = 1$, and to better match the data, they chose the following parameters: $\overline{g}_{Na} = 120mS/cm^2$, $\overline{g}_K = 34mS/cm^2$, $\overline{g}_L = 0.26mS/cm^2$, $V_{Na} = 50mV$, $V_K = -77mV$ $V_L = -54.4mV$. Then we pick the initial values for $V(0) = -65mV$, $m(0) = 0.0529$, $h(0) = 0.5961$, and $n(0) = 0.3177$, from where $m_\infty(-65)$, $h_\infty(-65)$ and $n_\infty(-65)$. After that we composed this figure for Hodgkin-Huxley Model under giant squid axon.

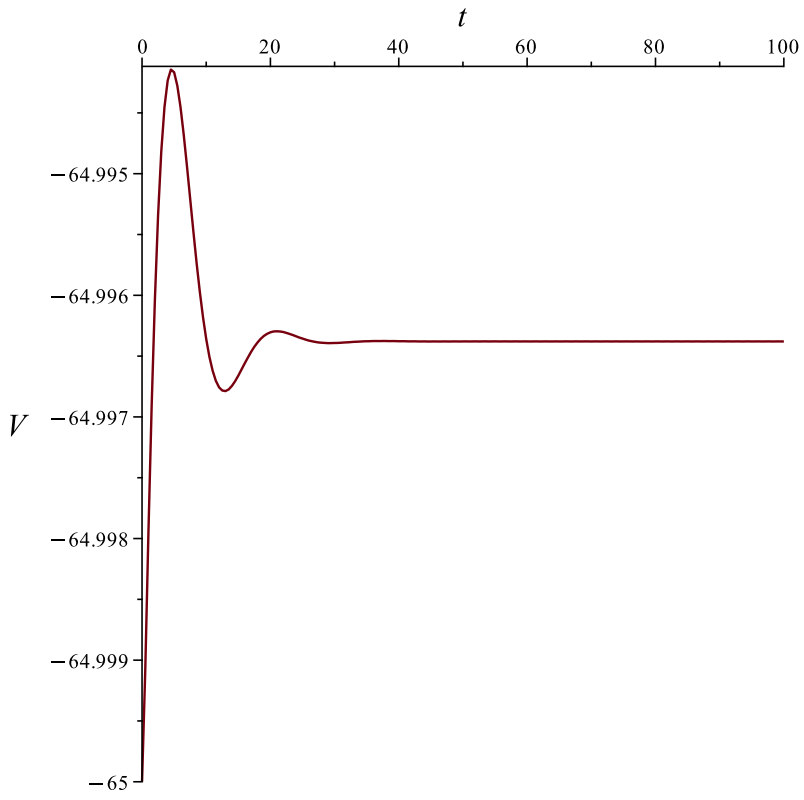

Figure 2.2: Hodgkin-Huxley Model

The plot shows a sharp, brief spike where the voltage rapidly depolarizes from approximately -65 mV and then quickly repolarizes. This is characteristic of an action potential, a fundamental feature of neuronal communication. The peak of the spike reaches just below -64.995 mV and returns almost to the baseline, suggesting a very short and rapid action potential. Following the spike, there is a noticeable dip below the baseline level, which is a typical feature after an action potential known as afterhyperpolarization. This occurs due to the opening of additional potassium channels, allowing more potassium ions to exit the neuron, which drives the inside of the cell to become more negative than the resting potential. After the afterhyperpolarization, the voltage gradually returns to a stable level, very close to where it started. This stabilization is likely due to the closing of the potassium channels and the activity of sodium-potassium pumps restoring the resting potential. The overall behavior shown in the plot suggests a single neuronal firing followed by the typical processes that reset the neuron's membrane potential to prepare it for potentially another action potential. The scale of the time axis and the voltage scale focused around a narrow range, highlighting the precision of the measurement and the sensitivity of the neuron to small changes in membrane potential.

After obtaining the figure, our next step is to evaluate the model's steady state. To do this, we configure the system equations all to equal zero.

$$
\begin{aligned}
-\overline{g}_K n^4 (V - V_K) - \overline{g}_{Na} m^3 h (V - V_{Na}) - \overline{g}_l (V - V_l) &= 0, \\
\phi[\alpha_n(V) \cdot (1 - n) - \beta_n(V) \cdot n] &= 0, \\
\phi[\alpha_m(V) \cdot (1 - m) - \beta_m(V) \cdot m] &= 0, \\
\phi[\alpha_h(V) \cdot (1 - h) - \beta_h(V) \cdot h] &= 0.
\end{aligned}
$$

Therefore, we got the solution set for this system in steady state:

$$V = -64.99637933,$$

$$h = 0.5959941248,$$

$$m = 0.05295508679,$$

$$n = 0.3177323997.$$

The value of $V = -64.99637933$ is close to typical resting potentials of neurons, indicating a stable state. The value of $h = 0.5959941248$ means that a substantial portion of sodium channels are inactivated, further reducing sodium current. The low value of m indicates that very few sodium channels are in the activation state, which is consistent with the neuron being at or near its resting state, as the activation of sodium channels is primarily responsible for the rapid depolarization phase of the action potential. The value of $n = 0.3177323997$ would indicate significant fraction of potassium channels are open, stabilizing the membrane potential.

2.3 Morris-Lecar Model

The Morris-Lecar model, developed by Catherine Morris and Harold Lecar in the early 1980s, was originally designed to describe the dynamics of electrical activity in barnacle muscle fibers. It is a two dimensional reduction version of Hudgkin-Huxley Model. The model reduces the dynamics of the membrane potential to two main variables: the membrane potential itself and a single gating variable that controls the conductance of one of the ionic currents. This simplification makes the model more analytically tractable and easier to simulate computationally. The Morris-Lecar model was aimed at capturing the dynamics of cells where calcium conductance is significant in generating electrical activity. This contrasts with the squid giant axon studied by Hodgkin and Huxley, where sodium conductance is more relevant.

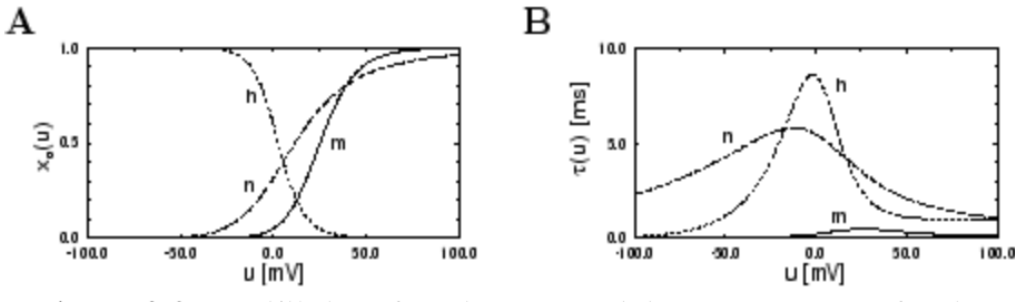

Figure 2.3: The Hodgkin-Huxley model, A. The equilibrium functions for the three variables m, n, h in the Hodgkin-Huxley model. B. The voltage-dependent time constant. The resting potential is at $u = -65mV$(arrow) and parameters are those given in previous chapters.[5]

u here is the same as V in previous chapters, represents the voltage. So we would like to keep using V. [4] For Figure 3.1, from graph A, it is obvious that $n_0(V)$ and $1 - h_0V$ are rather similar; in this case, we can approximate n, $1 - h$, by a single variable w. From a linear approximation, we can make two constant a, b such that $(b - h) \approx a \cdot n$. Then let

$$w = b - h = an \qquad m = m_0(V)$$

$$h = b - w \qquad \hat{w} = (\frac{w}{a})^4$$

$$n = \frac{w}{a} \qquad \hat{m_0}(V) = [m_0(V)]^3.$$

Morris and Lecar chose to use high voltage while they developed the model, and then they found the Na^+ channel closed under this situation. Therefore, they

modified the model,

$$\begin{aligned} C_M \frac{\partial V}{\partial t} &= I_{app} - g_k \cdot n^4(V - V_K) - g_{Na} \cdot m^3 h(V - V_{Na}) - g_L(V - V_L) \\ &= I_{app} - g_K \cdot (\frac{w}{a})^4(V - V_K) - g_{Na}[m_0(V)]^3(b - w)(V - V_{Na}) - g_L \cdot (V - V_L) \\ &= I_{app} - g_1 \cdot \hat{w}(V - V_1) - g_2 \cdot \hat{m}_0(V)(V - V_2) - g_L(V - V_L). \end{aligned}$$

Since they used calcium channel instead of sodium, and for consistency, they make a new n to replace $\hat{w}$ and $m_\infty(V)$ replaces $\hat{m}_0(V)$.

$$\begin{aligned} C_M \frac{\partial V}{\partial t} &= I_{app} - g_k \cdot n(V - V_K) - g_{Ca} \cdot m_\infty(V)(V - V_{Ca}) - g_L(V - V_L) \\ &\equiv I_{app} - I_{ion}(V, n), \\ \frac{\partial n}{\partial t} &= \phi(n_\infty(V) - n)/\tau_n(V), \end{aligned}$$

where,

$$\begin{aligned} m_\infty(V) &= \frac{1}{2}[1 + \tanh((V - V_1)/V_2)], \\ \tau_n(V) &= 1/\cosh((V - V_3)/(2V_4)), \\ n_\infty(V) &= \frac{1}{2}[1 + \tanh((V - V_3)/V_4)]. \end{aligned}$$

As the system evolves, n converges towards its equilibrium value, $n_\infty(V)$, at a rate determined by the reciprocal of the time, τ_n. And $\tau_n(V)$ is a function of the membrane potential, V, and characterizes the time scale on which n reaches equilibrium.

Chapter 3: Bifurcations for Morris-Lecar Model

The reason why people studying bifurcation is because bifurcation theory plays a crucial role in the analysis of mathematical models that mimic biological systems. Morris-Lacar model reduced the complexities from the Hodgkin-Huxley framework to refine the essence of voltage and current interactions across neuronal membranes. The usage of bifurcation analysis is to dissect the variety of neuronal responses to different stimuli.

At the heart of this analysis lie bifurcations: critical junctures where minor variations in parameters induce significant shifts in the system's long-term dynamics. Within the Morris-Lecar model, these pivotal moments mark the shift in neuronal activity, from a state of rest to continuous firing, or between different patterns of rhythmic activity. Altering key parameters—like the level of injected current, the conductance of ion channels, or the membrane's capacitance—can push the system through these bifurcations, transforming its behavior in fundamental ways.

The parameters for this model were derived empirically from experimental data. The process of determining these parameters involved careful experimentation and observation of the barnacle giant muscle fiber's electrical activity.

To identify the model parameters, Morris and Lecar first recorded the electrical responses of these muscle fibers to various stimuli. They then compared these recordings to the outputs of their mathematical model, which was based on the Hodgkin-Huxley formalism but simplified to make it more computationally tractable. By systematically varying the parameters in their model and evaluating how well the model's output matched the experimental data, they were able to hone in on the values that most accurately represented the biological processes at play.

Morris and Lecar adjusted these parameters to capture the essential features of the action potential and the resting state of the barnacle giant muscle fiber. It is important to note that while the model was originally developed for a specific type of muscle fiber, the methodology for parameter estimation is quite general and has been applied to neurons and other excitable cells.

The following is the table of parameters for such bifucation happens under different values of I_{app}.

Morris-Lecar parameters; the current, I_{app}, is a parameter [3]			
Parameter	Hopf	SNLC	Homoclinic
ϕ	0.04	0.067	0.23
g_{Ca}	4.4	4	4
V_3	2	12	12
V_4	30	17.4	17.4
V_{Ca}	120	120	120
V_K	-84	-84	-84
V_L	-60	-60	-60
g_K	8	8	8
g_L	2	2	2
V_1	-1.2	-1.2	-1.2
V_2	18	18	18
C_M	20	20	20

3.1 Hopf Bifurcation

The Hopf bifurcation is known for inducing limit cycles and spontaneous oscillations in a system as a specific parameter changes, reflecting rhythmic neuronal activities like firing patterns. This bifurcation is easier to mathematically analyze than SNLC bifurcations, offering a transparent view of the system's state changes. The emergent behaviors from a Hopf bifurcation matched the rhythmic behaviors observed in

barnacle muscle fibers, making it a fitting choice for biological modeling.

Studying Hopf bifurcation in the Morris-Lecar model is important for understanding how changes in system parameters can lead to the start of oscillatory behavior in neurons and other excitable cells. Neurons exhibit oscillatory activity, which is crucial for functions such as timing, signaling, and frequency modulation in the brain. Oscillations can arise due to intrinsic properties of the neuron or through interactions with other cells. Hopf bifurcation is a critical mathematical concept that explains how equilibrium points of a system can become unstable and give rise to periodic oscillations. In the context of the Morris-Lecar model, a Hopf bifurcation occurs when the parameter I_{app} crosses a certain threshold value. This bifurcation marks the transition from a non-oscillating state to a region where the neuron starts exhibiting rhythmic, cyclic activity. Understanding this transition is key to deciphering how neurons respond to various stimuli and conditions. For example, understanding when a neuron might switch from a resting state to repetitive firing can help in developing better treatments for neurological disorders such as epilepsy, where unwanted oscillatory activity leads to seizures.

We then would like to find out at which value of applied current emerges the Hopf bifurcation in Morris-Lecar System. We choose the parameter $I_{app} = 60, 90, 92, 95$.

We first test for $I_{app} = 60$ and configure the system equations to all equal zero.

$$C_M \frac{\partial V}{\partial t} = I_{app} - g_k \cdot n(V - V_K) - g_{Ca} \cdot m_\infty(V)(V - V_{Ca}) - g_L(V - V_L)$$

$$20\frac{\partial V}{\partial t} = 60 - 8 \cdot n(V + 84) - 4.4 \cdot \frac{1 + \tanh((V + 1.2)/18)}{2} \cdot (V - 120) - 2(V + 60)$$

$$= 0$$

$$\frac{\partial n}{\partial t} = \phi(n_\infty(V) - n)/\tau_n(V)$$

$$\frac{\partial n}{\partial t} = 0.04 \cdot (\frac{1 + \tanh((V - 2)/30)}{2} - n)/\frac{1}{\cosh((V - 2)/60)}$$

$$= 0.$$

Therefore, we got the solution set for this system in steady state:

$$V = -36.75474152, n = 0.07019815700$$

These values indicate that at steady state, the membrane potential V is approximately -36.75 mV, and the gating variable n is approximately 0.07. This specific steady state is likely a resting state of the neuron where there is no net current flowing across the membrane, meaning that the ionic currents through the different channels and the leak current balance the applied current. In the phase space, these values would correspond to an equilibrium point. Depending on the parameters of the model and the nature of this equilibrium point, it can either be stable (attracting nearby trajectories) or unstable (repelling them). To determine stability, one would usually perform a linear stability analysis around the equilibrium point by calculating the Jacobian matrix and its eigenvalues at this point.

$$\begin{bmatrix} \frac{\partial}{\partial V} - \frac{60+10V+40n(V+84)-11(1+\tanh(\frac{V+1.2}{18}))(V-120)}{100} & \frac{\partial}{\partial n} - \frac{60+10V+40n(V+84)-11(1+\tanh(\frac{V+1.2}{18}))(V-120)}{100} \\ \frac{\partial}{\partial V} 0.04(0.5 + 0.5\tanh(\frac{V-2}{30}) - n)\cosh(\frac{V-2}{60}) & \frac{\partial}{\partial n} 0.04(0.5 + 0.5\tanh(\frac{V-2}{30}) - n)\cosh(\frac{V-2}{60}) \end{bmatrix}$$

$$\downarrow$$

$$\begin{bmatrix} -\frac{35+40n+22(\frac{1-\tanh(\frac{V+1.2}{18})^2}{36})(V-120)-11\cdot\tanh(\frac{V+1.2}{18})}{100} & -\frac{2V+168}{5} \\ \frac{(1-\tanh(\frac{V-2}{30})^2)\cosh(\frac{V-2}{60})+(\frac{1+\tanh\frac{(V-2)}{30}}{2}-n)\cdot sinh(\frac{V-2}{60})}{1500} & -\frac{\cosh(\frac{V-2}{60})}{25} \end{bmatrix}$$

Now let's plug in the equilibrium point $(-36.75474152, 0.07019815700)$ and see if it is stable. Then the matrix becomes

$$\begin{bmatrix} -0.0612505032 & -18.89810339 \\ 0.0002116423128 & -0.04863821692 \end{bmatrix}$$

From this, we can find the eigenvalues are:

$$\begin{bmatrix} -0.0549443600600000 + 0.0629275048582967i \\ -0.0549443600600000 - 0.0629275048582967i \end{bmatrix}$$

Then we compose the vector field to the $I_{app} = 60$, we can see from the Figure 3.1 that there exists only one equilibrium which is stable and global attracted.

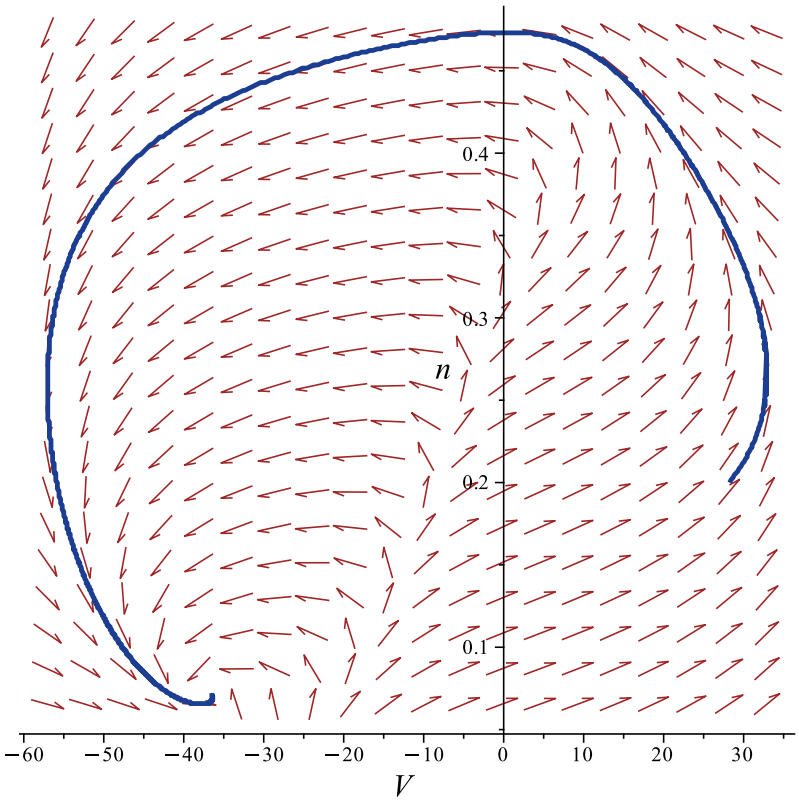

Figure 3.1: The blue curve is the trajectory starting at around $(28, 0.2)$, and is approaching the unique equilibrium point.

Next we are testing $I_{app} = 90$.

$$C_M \frac{\partial V}{\partial t} = I_{app} - g_k \cdot n(V - V_K) - g_{Ca} \cdot m_\infty(V)(V - V_{Ca}) - g_L(V - V_L)$$

$$20\frac{\partial V}{\partial t} = 90 - 8 \cdot n(V + 84) - 4.4 \cdot \frac{1 + \tanh((V + 1.2)/18)}{2} \cdot (V - 120) - 2(V + 60)$$

$$= 0$$

$$\frac{\partial n}{\partial t} = \phi(n_\infty(V) - n)/\tau_n(V)$$

$$\frac{\partial n}{\partial t} = 0.04 \cdot (\frac{1 + \tanh((V - 2)/30)}{2} - n)/\frac{1}{\cosh((V - 2)/60)}$$

$$= 0.$$

Therefore, we got the solution set for this system in steady state:

$$V = -26.59686698, n = 0.1293793233,$$

with the same process, we find out the differentiate matrix,

$$\begin{bmatrix} -\frac{21+40n+22(\frac{1-\tanh(\frac{V+1.2}{18})^2}{36})(V-120)-11\cdot\tanh(\frac{V+1.2}{18})}{100} & -\frac{2V+168}{5} \\ \frac{(1-\tanh(\frac{V-2}{30})^2)\cosh(\frac{V-2}{60})+(\frac{1+\tanh\frac{(V-2)}{30}}{2}-n)\cdot sinh(\frac{V-2}{60})}{1500} & -\frac{\cosh(\frac{V-2}{60})}{25} \end{bmatrix}.$$

After plug in the equilibrium point we have

$$\begin{bmatrix} 0.02581997233 & -22.96125321 \\ 0.0003351416123 & -0.04462988432 \end{bmatrix}.$$

The eigenvalues are:

$$\begin{bmatrix} -0.00940495599500000 + 0.0803397525869140i \\ -0.00940495599500000 - 0.0803397525869140i \end{bmatrix}$$

Then we compose the vector field to the $I_{app} = 90$,

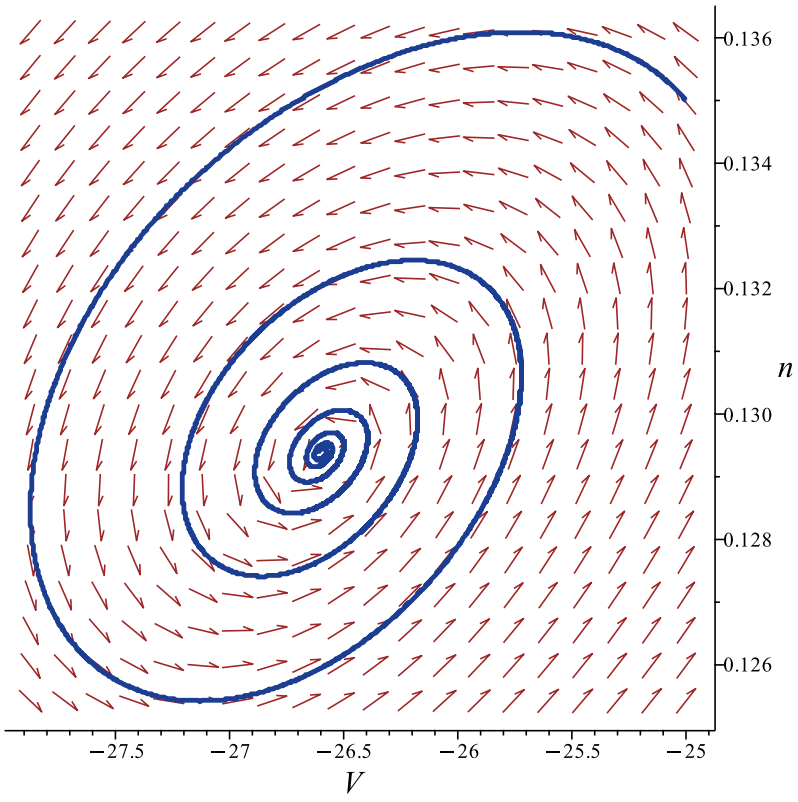

Figure 3.2: The blue curve is the trajectory starting at around $(-25, 0.135)$, and is approaching the unique equilibrium point.

we can see from the graph that there exist one equilibrium which is stable and global attracted.

Next we are testing $I_{app} = 92$.

$$C_M \frac{\partial V}{\partial t} = I_{app} - g_k \cdot n(V - V_K) - g_{Ca} \cdot m_\infty(V)(V - V_{Ca}) - g_L(V - V_L)$$

$$20\frac{\partial V}{\partial t} = 92 - 8 \cdot n(V + 84) - 4.4 \cdot \frac{1 + \tanh((V + 1.2)/18)}{2} \cdot (V - 120) - 2(V + 60)$$

$$= 0$$

$$\frac{\partial n}{\partial t} = \phi(n_\infty(V) - n)/\tau_n(V)$$

$$\frac{\partial n}{\partial t} = 0.04 \cdot (\frac{1 + \tanh((V - 2)/30)}{2} - n)/\frac{1}{\cosh((V - 2)/60)}$$

$$= 0.$$

Therefore, we got the solution set for this system in steady state:

$$V = -25.91198391, n = 0.1346099577,$$

with the same process, we find out the differentiate matrix,

$$\begin{bmatrix} -\frac{21+40n+22(\frac{1-\tanh(\frac{V+1.2}{18})^2}{36})(V-120)-11\cdot\tanh(\frac{V+1.2}{18})}{100} & -\frac{2V+168}{5} \\ \frac{(1-\tanh(\frac{V-2}{30})^2)\cosh(\frac{V-2}{60})+(\frac{1+\tanh\frac{(V-2)}{30}}{2}-n)\cdot sinh(\frac{V-2}{60})}{1500} & -\frac{\cosh(\frac{V-2}{60})}{25} \end{bmatrix}.$$

After plug in the equilibrium point we have

$$\begin{bmatrix} 0.03507011157 & -23.23520644 \\ 0.0003448638434 & -0.04440683712 \end{bmatrix}.$$

The eigenvalues are:

$$\begin{bmatrix} -0.00466836277500000 + 0.0802111977957106i \\ -0.00466836277500000 - 0.0802111977957106i \end{bmatrix}$$

Then we compose the vector field to the $I_{app} = 92$,

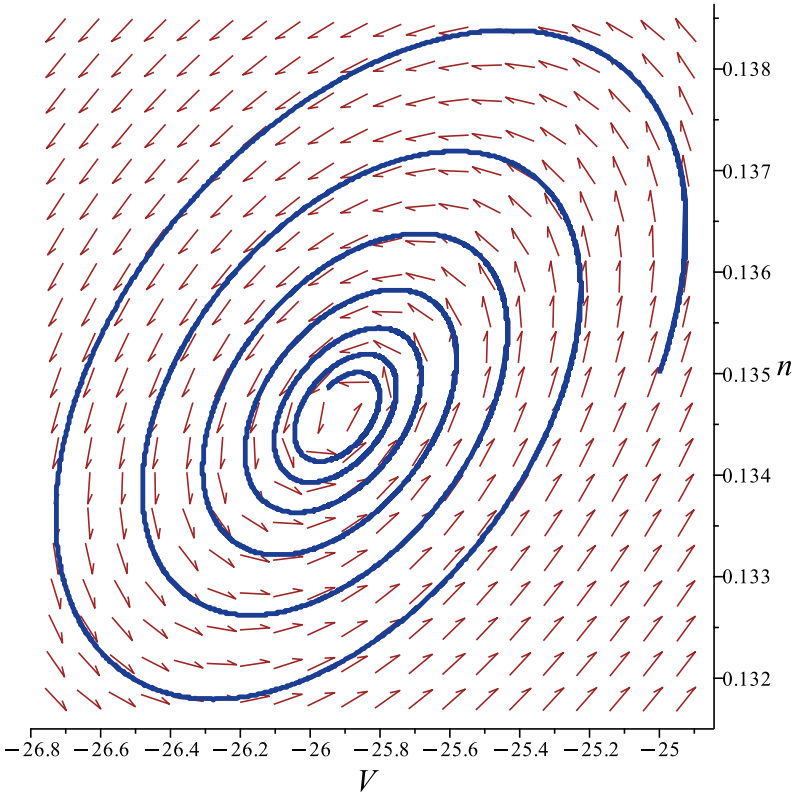

Figure 3.3: The blue curve is the trajectory starting at around $(-25, 0.135)$, and is approaching the unique equilibrium point.

we can see from the Figure 3.3 that it is similar to $I_{app} = 90$, there is also exist one equilibrium. However, we can see from the graphs, the equilibrium is becoming weaker.

Lastly, we test for $I_{app} = 95$.

$$C_M \frac{\partial V}{\partial t} = I_{app} - g_k \cdot n(V - V_K) - g_{Ca} \cdot m_\infty(V)(V - V_{Ca}) - g_L(V - V_L)$$

$$20\frac{\partial V}{\partial t} = 95 - 8 \cdot n(V + 84) - 4.4 \cdot \frac{1 + \tanh((V + 1.2)/18)}{2} \cdot (V - 120) - 2(V + 60)$$

$$= 0$$

$$\frac{\partial n}{\partial t} = \phi(n_\infty(V) - n)/\tau_n(V)$$

$$\frac{\partial n}{\partial t} = 0.04 \cdot (\frac{1 + \tanh((V - 2)/30)}{2} - n)/\frac{1}{\cosh((V - 2)/60)}$$

$$= 0.$$

Therefore, we got the solution set for this system in steady state:

$$V = -24.87209187, n = 0.1428922499,$$

with the same process, we find out the differentiate matrix,

$$\begin{bmatrix} -\frac{21+40n+22(\frac{1-\tanh(\frac{V+1.2}{18})^2}{36})(V-120)-11\cdot\tanh(\frac{V+1.2}{18})}{100} & -\frac{2V+168}{5} \\ \frac{(1-\tanh(\frac{V-2}{30})^2)\cosh(\frac{V-2}{60})+(\frac{1+\tanh\frac{(V-2)}{30}}{2}-n)\cdot sinh(\frac{V-2}{60})}{1500} & -\frac{\cosh(\frac{V-2}{60})}{25} \end{bmatrix}.$$

After plug in the equilibrium point we have

$$\begin{bmatrix} 0.05009449381 & -23.65116325 \\ 0.0003599041050 & -0.04407922628 \end{bmatrix}.$$

The eigenvalues are:

$$\begin{bmatrix} 0.00300763376500001 + 0.0793408996218389i \\ 0.00300763376500001 - 0.0793408996218389i \end{bmatrix}$$

As we can see from the eigenvalues, at this point, the real parts become positive. Now we compose the vector field to the $I_{app} = 95$,

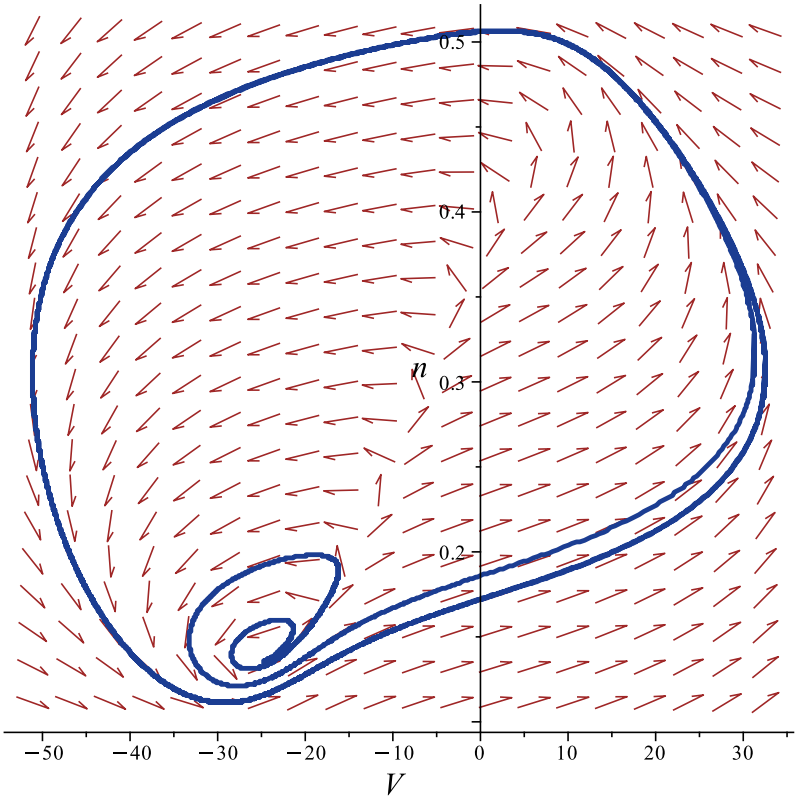

Figure 3.4: The blue curve is the trajectory starting near the equilibrium, and is approaching the limit cycle that arise.

It is a little bit hard to see the pattern of limit cycle, we would like to show another phase portrait for $I_{app} = 95$ from a point outside of limit cycle and see it pattern.

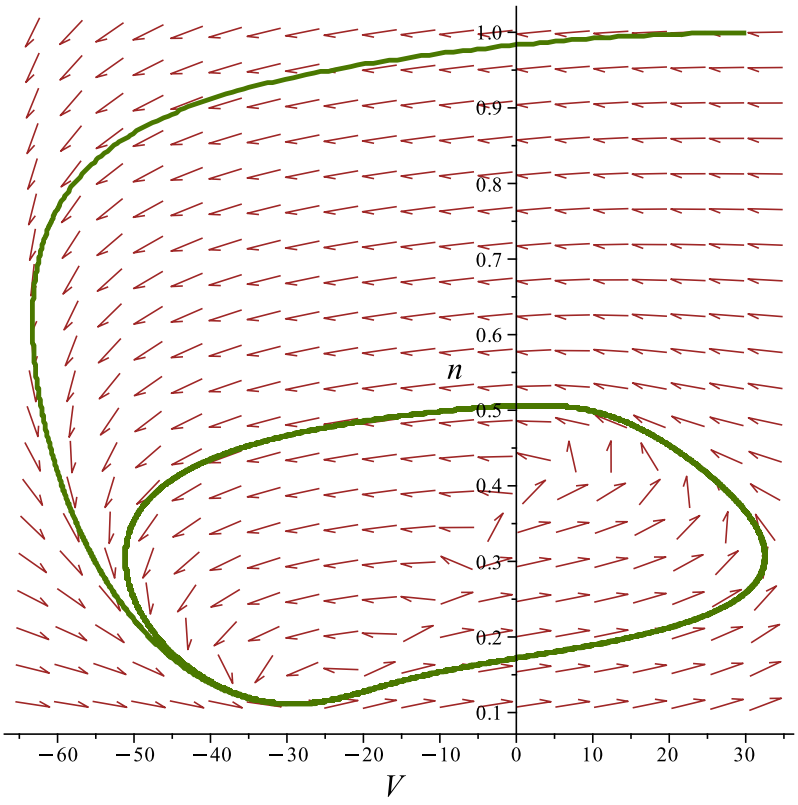

Figure 3.5: Vector Field For Morris-Lecar Model Under I_{app}=95 From A Point Outside Of The Limit Cycle

Then we would like to combine these two graphs to see if they are both going to

same limit cycle.

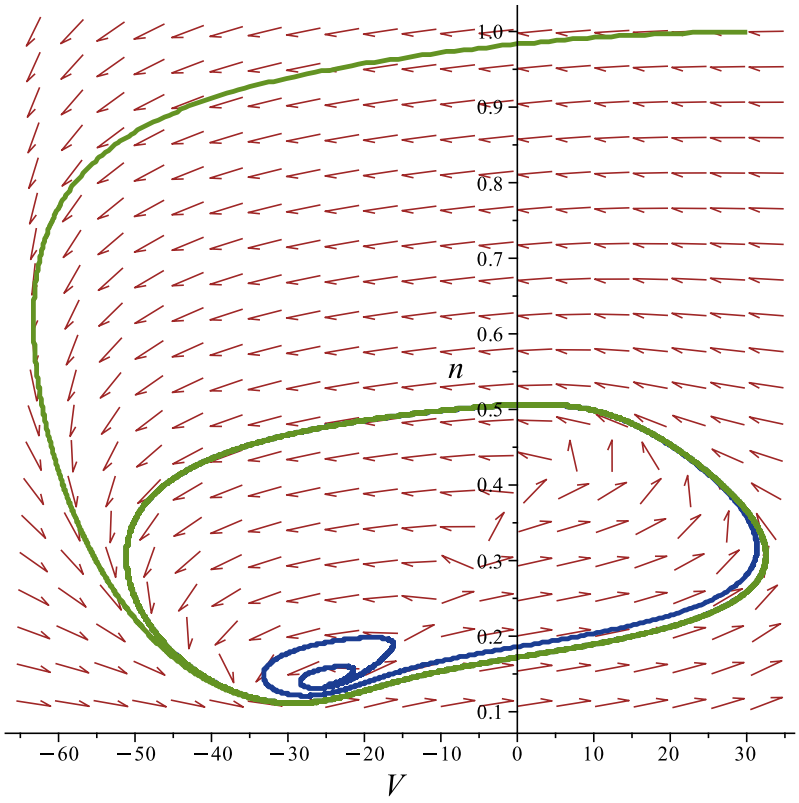

Figure 3.6: Vector Field for Morris-Lecar Model Under I_{app}=95

From Figure 3.6, we can see that there exists one stable and one unstable.

In conclusion, with all these phase portraits under different parameters, we can conclude that the Hopf bifurcation happened between $I_{app} = 92 \text{and} 95$. Another way to see this pattern is from the real part of the eigenvalues, for $I_{app} = 60, 90, 92$, they are getting close to 0 from negative, and then comes to positive as we can see at

$I_{app} = 95$. Therefore, in between 92 to 95, when the real part of eigenvalue is 0, the Hopf bifurcation appears.

3.2 SNLC Bifurcation

Saddle-Node on Limit Cycle (SNLC) bifurcation offers a delicate approach to understanding neuronal dynamics, presenting a steady progression from equilibrium to cyclical activity. They properly simulate neurons' gradual shift from a dormant state to active firing with increasing stimulus, a process that mirrors natural biological responses where oscillatory activity initiates at an undetectably slow rate. As system parameters evolve, these oscillations gain a discernible period, which subtly accelerates. The resilience of SNLC bifurcations to shifts in system parameters and external disturbances makes them especially valuable for depicting the functionality of biological systems, which are frequently subjected to variable and unpredictable conditions. They adeptly represent neurons' tonic firing behavior, capturing the slow onset of action potentials as stimuli cross specific thresholds, followed by a steady increase in firing rate corresponding to the stimulus intensity. This characteristic is instrumental for modeling neurons that exhibit gradual, as opposed to sudden, transitions into rhythmic firing, unlike the immediate oscillations induced by Hopf bifurcations.

Studying a saddle-node on limit cycle bifurcation in the Morris-Lecar model is significant for several reasons, particularly in understanding the dynamics of neuronal behavior under varying conditions. A saddle-node on limit cycle bifurcation occurs when a limit cycle appears or disappears as a parameter is varied. In the context of neuronal models like Morris-Lecar, this type of bifurcation helps explain how neurons can abruptly transition between different states of activity, such as from no firing to regular firing or from regular firing to bursting. This bifurcation

describes situations where small changes in parameters can cause significant qualitative changes in the behavior of neurons. It helps in understanding the thresholds beyond which neurons change their firing patterns, which is crucial for modeling how neurons respond to synaptic inputs or changes in their intrinsic properties. This is particularly useful in understanding and predicting the behavior of neurons under different pharmacological influences or in different disease states.

With the similar steps as we did for hopf bifurcation, we would like to find out the value of I_{app} where the SNLC bifurcation occurs. We first briefly find out the range that bifurcation happens, and then narrow down.

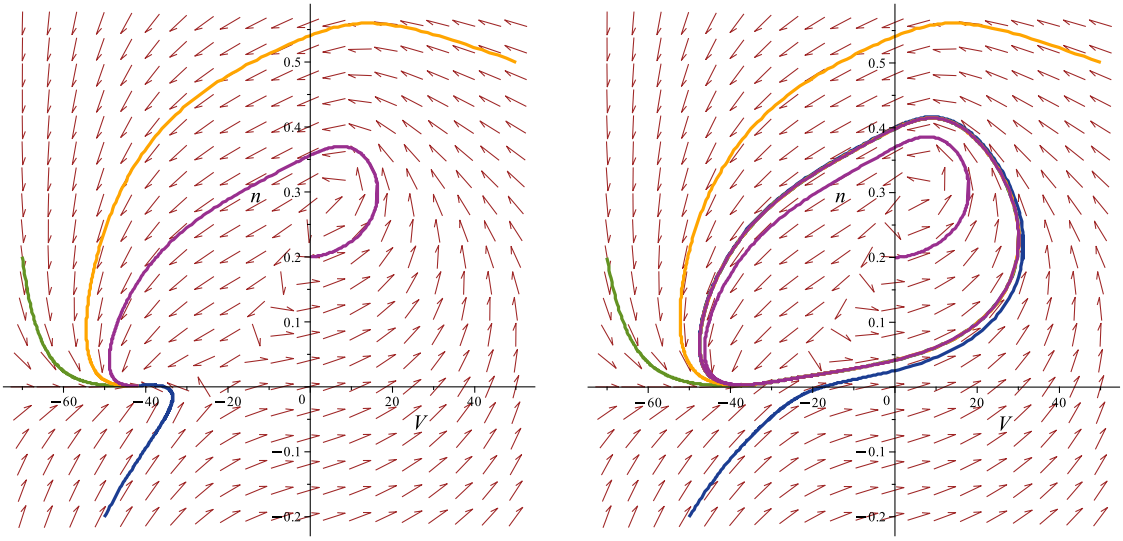

Figure 3.7: On the left hand side is the phase portrait at $I_{app} = 30$. On the right hand side is the phase portrait at $I_{app} = 40$

As we can see from Figure 3.7, at $I_{app} = 30$, we tested trajectories with three different initial values. Two of them are located at left bottom, the points approximately are $(-40, 0)$ and $(-22, -0.02)$. And the last one is located around $(3.8, 0.28)$. All three trajectories approach the equilibrium at $(-31, 0.01)$ which appears to be a global attractor with negative real part of eigenvalues. For the $I_{app} = 40$, the bottom two starting points approach the equilibrium at $(-22, 0.03)$ which is the continuation of the previous equilibrium for $I_{app} = 30$, and a limit cycle has formed and attracts the trajectory colored in purple. This figure implies that the SNLC bifurcation happened in between 30 to 40. Therefore, we would like to pick values at middle and see the patterns.

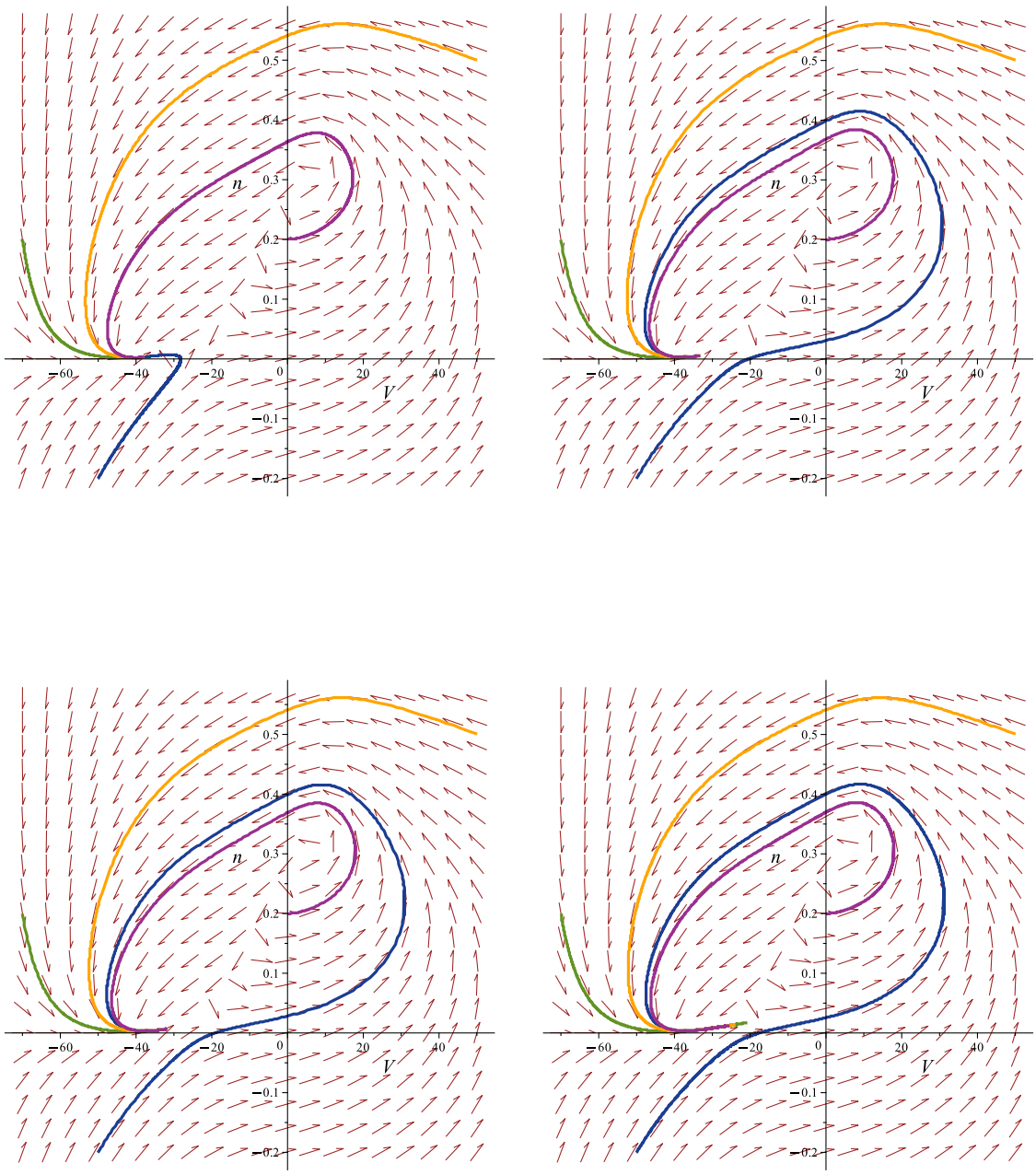

Figure 3.8: On the upper left is the phase portrait at $I_{app} = 35$. On the upper right is the phase portrait at $I_{app} = 38.75$. On the bottom left is the phase portrait at $I_{app} = 39.375$. On the bottom right is the phase portrait at $I_{app} = 39.996$.

We can see from Figure 3.8, from $I_{app} = 38.75$ to $I_{app} = 39.996$ are all look the same, in which all the trajectories are appoaching to same equilibrium point at the bottom left. Therefore, we would like to pick a value in between 39.996 and 40 to see the change of phase portraits.

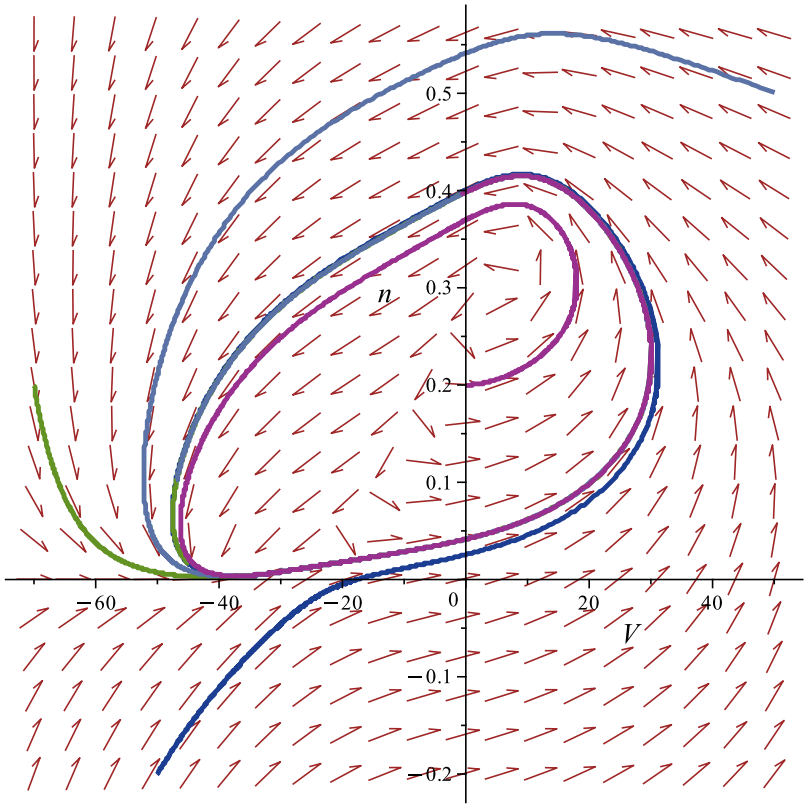

Figure 3.9: Phase Portrait at $I_{app} = 39.997$

From Figure 3.9, we can see the purple trajectory approaching a limit cycle. Therefore, we can conclude that the SNLC bifurcation happens between $I_{app} = 39.996$ and $I_{app} = 39.997$.

Chapter 4: Applications and future direction to math neuroscience

Mathematical neuroscience leverages models like the Hodgkin-Huxley, Morris-Lecar, and FitzHugh-Nagumo to decipher complex neural phenomena and forecast future developments in the field. These models serve as fundamental tools for understanding how neurons communicate, process information, and contribute to larger neural network functions.

Looking to the future, the convergence of mathematical models spans several promising directions. These include multiscale modeling to understand interactions across molecular, cellular, and network levels within the brain, and the integration of machine learning to refine models and interpret expansive neural datasets, leading to more accurate neural behavior predictions. Adaptive models could be incorporated into real-time closed-loop control systems for applications like deep brain stimulation. Moreover, the exploration of quantum biophysics could herald new vistas in mathematical neuroscience. Insights gleaned from these models are also propelling advancements in neuromorphic computing and synthetic biology, enabling the construction of biological circuits with specified functionalities and the development of neuromorphic chips that simulate neural processing.

Bibliography

[1] Julie Bumbaugh. "A dynamical system study of the Hodgkin-Huxley Model of nerve membrane". PhD thesis. 2012.

[2] Alain Destexhe and John R Huguenard. "Nonlinear thermodynamic models of voltage-dependent currents". In: *Journal of computational neuroscience* 9 (2000), pp. 259–270.

[3] Bard Ermentrout and David Hillel Terman. *Mathematical foundations of neuroscience*. Vol. 35. Springer, 2010.

[4] Wulfram Gerstner and Werner M Kistler. *Spiking neuron models: Single neurons, populations, plasticity*. Cambridge university press, 2002.

[5] Wulfram Gerstner et al. *Neuronal dynamics: From single neurons to networks and models of cognition*. Cambridge University Press, 2014.

[6] Oliver Heaviside. *Electrical papers*. Vol. 2. Cambridge University Press, 2011.

[7] Alan L Hodgkin and Andrew F Huxley. "A quantitative description of membrane current and its application to conduction and excitation in nerve". In: *The Journal of physiology* 117.4 (1952), pp. 500–544.

[8] Daniel Johnston and Samuel Miao-Sin Wu. *Foundations of cellular neurophysiology*. MIT press, 1994.

[9] George Marmont. "Studies on the axon membrane. I. A new method". In: *Journal of cellular and comparative physiology* 34.3 (1949), pp. 351–382.

[10] George Marmont. "Studies on the axon membrane. I. A new method". In: *Journal of cellular and comparative physiology* 34.3 (1949), pp. 351–382.

[11] P Waage and CM Guldberg. "Studier over affiniteten". In: *Forhandlinger i Videnskabs-selskabet i Christiania* 1 (1864), pp. 35–45.

Scarlett (Shiyi) Lyu

scarlettlyu7@gmail.com | 743-649-1198

EDUCATION

Wake Forest University Winston-Salem, NC

Master of Science in Mathematics GPA: 3.3/4.0 Expected Aug 2024

University of California - Irvine Irvine, CA

Bachelor of Science in Mathematics GPA: 3.4/4.0 Aug. 2019 - Mar. 2022

RELEVANT COURSEWORK

(Graduate level) Advanced Abstract Algebra, Topology, Real Analysis, Optimization with Numerical Method

(Undergraduate level) Elliptic Curves, Complex Analysis, Real Analysis, Modern Geometry, Differential Geometry, Probability, Discrete Dynamical System, Number Theory, Group Theory, Advanced Linear Algebra

RESEARCH EXPERIENCE

Mathematical Neuroscience Jun. 2023 - Present

Research Advisor : Miaohua Jiang, WFU Department of Mathematics

- Investigated and computed the invariant subrings of a Hopf algebra within the context of iterated Ore extensions.
- Developed mathematical models to articulate the relationships involved, utilizing Maple for implementation.
- Analyzed and interpreted the mathematical models to draw meaningful conclusions.
- Authored a comprehensive research article using LaTeX, outlining the findings and contributions.

Geometry Discovery Project (GDP) Dec. 2021 - Jun. 2022

Research Advisor : Zhiqin Lu, University of California - Irvine, Department of Mathematics

- Conducted in-depth research in classical Euclidean geometry and triangle geometry, actively participating in weekly discussions to enhance understanding.
- Designed and curated website content encompassing over 40 topics, including advanced concepts like Isogonal Conjugate, Isotomic Conjugate Points, and the Miquel Point.
- Tailored content specifically for high school students, aiming to prepare them for AMC and other mathematical competitions.
- Authored and published over 60 pages of educational material using LaTeX, offering comprehensive insights and step-by-step explanations for geometric processes. Topics covered include 3, 5, 7, 20, and 25.

Optimization and Linear Programming Research Jun. 2021 - Dec. 2021

Research Advisor : Ming Gu, University of California - Berkeley, Department of Mathematics

- Conducted comprehensive research on various mathematical problems, including diet optimization, two-person zero-sum games, and transportation problems.
- Actively participated in project discussions, employing Linear Programming Basics and the Simplex Method for optimization coding. The Simplex Method To Optimize Food Supply Published at the 2022 2nd International Conference on Applied Mathematics, Modelling, and Intelligent Computing.

SCHOLARSHIP

Teaching Assistant With Tuition Remission Jul. 2022 - Present

Teaching and Working Experience

Teacher Assistant WFU Math and Stats Center Aug. 2022 - Present

- Led weekly study sessions for groups of 5 or more students, adeptly managing group dynamics and addressing individual needs.
- Evaluated and provided constructive feedback on the work of more than 100 students, spanning two weekly assignments and five sections of math courses.
- Collaborated with faculty members to design homework assignments and lectures, enhancing the learning experience.
- Offered support to students of concern through weekly one-on-one in-person meetings, demonstrating a commitment to student well-being.
- Composed detailed weekly work summaries to inform faculty and students about ongoing progress and challenges.

Math Tutor UC Irvine CalTeach Department Aug. 2021 - Mar. 2022

- Instructed students in elementary courses, including linear algebra and elementary analysis, utilizing online platforms such as Zoom and Gather Town.
- Conducted four weekly lectures, engaging undergraduates by addressing their questions and fostering interactive learning experiences.
- Effectively translated complex theories into comprehensible ideas, breaking down intricate concepts into easily understandable components.
- Composed detailed weekly work summaries to inform faculty and students about ongoing progress and challenges.

CONFERENCES and WORKSHOPS

TriCAMS	Duke University	Nov. 2023
TAGMaC	North Carolina State University	Sep. 2023
TAGMaC	Duke University	Feb. 2023
GROW 2021	online, Duke University	Oct. 2021

PUBLICATIONS

Xiaoyi Ji, Shiyi Lyu, *The Simplex Method To Optimize Food Supply*, 2022 2nd International Conference on Applied Mathematics, Modelling and Intelligent Computing (Accepted and invited to give an oral report in CAMMIC 2022)

REFERENCES

Zhiqin Lu

Professor

Department of Mathematics

University of California - Irvine

Email: zlu@uci.edu

Miaohua Jiang

Professor

Department of Mathematics

Wake Forest University

Email: jiangm@wfu.edu

Jacob Mayle

Teacher-Scholar Postdoctoral Fellow

Department of Mathematics

Wake Forest University

Email: maylej@wfu.edu